

1    **TITLE**

2

3    **ISG15/USP18/STAT2 is a molecular hub regulating autocrine IFN I-  
4    mediated control of Dengue and Zika virus replication**

5

6    Constanza Eleonora Espada<sup>1</sup>, Edroaldo Lummertz da Rocha<sup>1</sup>, Adara Aurea  
7    dos Santos<sup>1</sup>, Zamira Guerra Soares<sup>1</sup>, Greicy Malaquias<sup>1</sup>, Daniel Oliveira  
8    Patrício<sup>1</sup>, Edgar Gonzalez Kozlova<sup>1</sup>, Paula Fernandes dos Santos<sup>1</sup>, Juliano  
9    Bordignon<sup>2</sup>, Thomas J. Sanford<sup>3</sup>, Teodoro Fajardo<sup>3</sup>, Trevor R. Sweeney<sup>3</sup>,  
10   André Báfica<sup>1</sup>, Daniel Santos Mansur<sup>1\*</sup>

11

12    <sup>1</sup>Laboratório de Imunobiologia, Departamento de Microbiologia, Imunologia e  
13    Parasitologia, Centro de Ciências Biológicas, Universidade Federal de Santa  
14    Catarina, Santa Catarina CEP 88040-900, Brazil.

15

16    <sup>2</sup>Laboratório de Virologia Molecular, Instituto Carlos Chagas, ICC/Fiocruz-PR,  
17    Curitiba, Paraná, CEP 81350-010, Brazil.

18

19    <sup>3</sup>Division of Virology, Department of Pathology, University of Cambridge,  
20    Addenbrooke's Hospital, Hills Road, Cambridge, CB2 0QQ, UK.

21

22    \*Correspondence: daniel.mansur@ufsc.br

23

24    **SUMMARY**

25

26    The establishment of a virus infection is the result of the pathogen's ability to  
27    replicate in a hostile environment generated by the host's immune system.  
28    Here, we found that ISG15 restricts Dengue and Zika viruses' replication  
29    through the stabilization of its binding partner USP18. ISG15 expression was  
30    necessary to control DV replication driven by both autocrine and paracrine  
31    type one interferon (IFN-I) signaling. Moreover, USP18 competes with NS5-  
32    mediated STAT2 degradation, a major mechanism for establishment of  
33    flavivirus infection. Strikingly, reconstitution of USP18 in ISG15-deficient cells  
34    was sufficient to restore the cells' immune response and restrict virus growth,

35 suggesting that the IFNAR-mediated ISG15 activity is also antiviral. Our  
36 results add a novel layer of complexity in the virus/host interaction interface  
37 and suggest that NS5 has a narrow window of opportunity to degrade STAT2,  
38 therefore suppressing host's IFN-I mediated response and promoting virus  
39 replication.

40

## 41 **KEYWORDS**

42 Dengue virus, Zika virus, ISG15, USP18, type one interferon, ISGylation,  
43 antiviral response, immune evasion, NS5, STAT2

44

## 45 **INTRODUCTION**

46

47 Cells detect infection by recognizing molecular patterns derived from  
48 pathogen's constituents (PAMPs) or cell damage (DAMPs). During viral  
49 infection, nucleic acid is a major signal that triggers the innate immune  
50 response, inducing a type one interferon (IFN-I)-mediated antiviral state (1, 2).  
51 IFN-I binds to its cognate receptor and activates the JAK/STAT pathway,  
52 leading to expression of hundreds of interferon stimulated genes (ISGs) that  
53 make the intracellular environment hostile to viral replication in infected and  
54 proximal cells (3). The evolutionary arms race between viruses and its hosts  
55 led to evolution of immune evasion mechanisms that are crucial for successful  
56 viral replication. Considering IFN-I's importance in viral infection control, many  
57 immunomodulatory proteins target this signaling pathway (4).

58 Several flaviviruses, such as dengue virus (DV), Zika virus (ZIKV) and yellow  
59 fever virus (YFV), have emerged and re-emerged over recent years and are  
60 the leading cause of human arbovirus infection (5, 6). DV alone infects nearly  
61 400 million people every year (7) with extensive health and economic burden  
62 (8). A requirement for effective flavivirus emergence is the ability to counteract  
63 the human immune system.

64 The compact flavivirus genome encodes seven non-structural proteins that  
65 are responsible for viral replication and immune evasion. Six of these proteins  
66 are not secreted implying that intracellular pathways are central targets for  
67 evasion (9–13). For instance, DV non-structural protein 5 (NS5), which is the  
68 viral RNA-dependent-RNA-polymerase (RdRp) and a methyltransferase,

69 mediates STAT2 degradation by facilitating its interaction with UBR4, leading  
70 to its ubiquitination and subsequent proteasomal targeting (14). This evasion  
71 pathway is functional in humans but not mice due to differences in the amino  
72 acid sequence of human and murine STAT2 (15).

73 ISG15 is an intracellular and secreted ubiquitin-like protein that has three  
74 described functions. Extracellular ISG15 acts as a cytokine, leading to the  
75 expression of IFN $\gamma$  and IL-10 in diverse immune cells (16–18). It has been  
76 suggested that humans lacking ISG15 have severe mycobacterial disease  
77 due to deficiency in IFN $\gamma$  production by NK cells (19). Moreover, ISG15 mRNA  
78 is highly expressed in active tuberculosis and strongly correlates with disease  
79 severity (17, 20).

80 ISG15 is conjugated to other proteins through a three-step ubiquitination-like  
81 process (21) in which the main ligase for ISGylation is the HECT domain and  
82 RCC1-like domain-containing protein 5 (HERC5) (22, 23). ISGylated proteins  
83 are affected in several different ways, such as increased or reduced stability  
84 and activity. ISG15 can also be conjugated to viral proteins, impacting their  
85 function, and therefore belong in the plethora of ISGs with a direct antiviral  
86 function (3, 24).

87 The third and more recently described role of ISG15 is its IFN-I modulatory  
88 function. Non-conjugated ISG15 binds and stabilizes the ISG USP18, a  
89 protease that negatively regulates IFN-I signaling and also serves as a  
90 deISGylation protein (25–27). Correspondingly, individuals lacking ISG15 are  
91 prone to severe interferonopathies due to decreased USP18 function and  
92 increased IFN-I signaling. Interestingly, ISG15-deficient patients do not have  
93 enhanced susceptibility to viruses suggesting ISG15 is not necessary to  
94 control ubiquitous viral infections *in vivo* (28). In contrast to the indirect role of  
95 ISG15 in negative regulation of IFN-I signaling through the USP18 axis in  
96 humans (28, 29), murine ISG15 itself blocks replication of human viruses such  
97 as Influenza and HSV-1(30). These findings implicate ISG15 as an important  
98 molecule inhibiting IFN-I-mediated actions but also suggest that ISG15 may  
99 mediate host cell intrinsic mechanisms triggered by viruses. However, how  
100 ISG15 bridges these apparently two paradoxical phenomena is unclear.

101 Specifically, it is possible that ISG15 directly regulates proteins exploited by  
102 viruses during early intracellular infection events.

103 Here, we observed that, unlike several other ISGs, ISG15 is highly expressed  
104 in infected cells containing the DV genome. Furthermore, independently of its  
105 ISGylation function, ISG15 restricts flavivirus replication primarily in the  
106 infected cell by stabilizing USP18, which in turn competes with viral NS5 for  
107 binding to STAT2. Our results suggest that flaviviruses exploit an ISG15-  
108 mediated IFN-I regulatory mechanism to evade innate immunity and enable  
109 replication.

110

111

## 112 RESULTS

113

### 114 *ISG15 is expressed in DV-infected cells*

115

116 The cell is a fundamental unit for viral infection control and developments in  
117 single-cell sequencing technology have enabled examination of host-  
118 pathogen interactions in great detail. Recently, Zanini and colleagues  
119 generated single-cell RNA sequencing data from two human cell lines  
120 (PBMCs and the HuH7 hepatoma cell line) independently infected with DV  
121 (31, 32). We re-analyzed available single-cell transcriptomic data dividing  
122 cells into three categories: uninfected, infected and bystander. Here we define  
123 uninfected cells as those derived from healthy donors, bystander cells as  
124 those derived from an infected patient or have been exposed to the virus but  
125 did not have the viral RNA detected and infected cells as those in which viral  
126 genome was detected. We used t-Distributed Stochastic Neighbor Embedding  
127 (tSNE) analysis to visualize cell-to-cell relationships in space of reduced  
128 dimensionality. As reported previously (31, 32), global cellular mRNA  
129 expression profiling was not sufficient to separate infected or bystander from  
130 uninfected cells, suggesting a high variability of gene expression in these  
131 samples (Figure 1A and S1A). As IFN-I are key elements in controlling  
132 infection, we filtered the results of the differential gene expression analysis  
133 using the gene ontology (GO) term for “type one interferon”. The Venn  
134 diagram in figure 1B shows that from the 394 differentially expressed (DE)

135 genes in peripheral blood mononuclear cells (PBMCs) of patients infected  
136 with DV or healthy donors, 37 were ISGs (IFN-I GO). ISG15, UBE2L6,  
137 HERC5 and USP18, members of the ISGylation pathway, were differentially  
138 expressed during DV infection (Figure 1C in bold). Interestingly, in contrast to  
139 other single cell experiments using Influenza virus as a model where all the  
140 members of the ISGylation pathway seem to be expressed at similar levels in  
141 both infected and bystander cells (33), HERC5 was the only member of the  
142 ISGylation pathway with a higher expression level in bystander cells (Figure  
143 1C and D). In the data set derived from the HuH7 cell line, ISG15 was the  
144 only canonical antiviral protein expressed in DV genome-containing cells  
145 (Figure S1C and D). This is in agreement with previous reports that the HuH7  
146 cell line does not produce IFN-I upon viral infection (34–36) and could explain  
147 the high number of infected cells (Figure S1A) in comparison with the number  
148 of infected PMBCs (Figure 1A). In PBMCs, NK, monocytes and B cells were  
149 the infected cells with higher ISG15 expression and similar to the data from  
150 Zanini and colleagues (32) B cells and monocytes being proportionately the  
151 most infected cells (Figure 1E). These results show that in contrast to most  
152 ISGs, ISG15 and other components of the ISGylation pathway are enriched in  
153 cells where the DV genome was present.

154

#### 155 *ISG15 restricts DV and ZIKV replication*

156

157 The enrichment of ISG15-related genes at a single-cell level led us to  
158 investigate how ISG15 might impact flavivirus replication in a human cell. We  
159 used an A549 cell line lacking ISG15, previously generated using  
160 CRISPR/Cas9 in our lab (17). A549 cells were chosen due to their ability to  
161 support flavivirus replication and most importantly to produce and respond to  
162 IFN-I (37–40).

163 ISG15-deficient cells were more susceptible to DV infection as shown by an  
164 increased plaque size (Figure 2A and B) and number of infected cells per  
165 plaque (Figure 2C). In addition, we determined the kinetics of DV replication  
166 and dissemination by using a low multiplicity of infection (MOI), to allow for  
167 viral spread through secondary infection events. Percentages of infected cells  
168 over time (Figure 2D), relative DV Pre-Membrane RNA quantification in the

169 supernatant (Figure 2E) and infectious particle formation (Figure 2F) were  
170 also increased in the absence of ISG15. DV infection at 4 °C for 2 hours  
171 followed by relative intracellular DV genome quantification indicated no  
172 differences in viral RNA between WT and knockout cells up to 48 hours post-  
173 infection (Figure 2G), indicating that ISG15 plays a role in the DV life cycle at  
174 a stage following viral entry. Importantly, reconstitution of ISG15 expression in  
175 knockout cells led to phenotypic reversion (Figure 2H and I), confirming that  
176 the effects observed in our experiments were caused by depletion of ISG15.  
177 Finally, lack of ISG15 expression led to an increase in plaque size in cells  
178 infected with a phylogenetically related virus, such as ZIKV (Figure 2J and K)  
179 but not with HSV-1 (Figure S2A and B) or VSV (Figure S2C and D). These  
180 results are in line with Speer and colleagues' data where cells isolated from  
181 humans deficient for ISG15 do not have enhanced susceptibility to HSV-1 or  
182 VSV (29). Altogether these results suggest a specific role for ISG15 in the  
183 regulation of flavivirus replication and dissemination.

184

185 *ISGylation deficiency does not affect DV spread*

186

187 ISG15 is an IFN-I-inducible ubiquitin-like molecule and can be conjugated to  
188 target proteins by HERC5, an ISG15 ligase also induced by IFN (23, 41). Of  
189 note, ISGylation of host or viral proteins was reported to inhibit replication of  
190 several viruses such as influenza (IAV) (42), human cytomegalovirus (HCMV)  
191 (43) and human respiratory syncytial virus (RSV) (44). Moreover, DV proteins  
192 were also shown to be ISGylated (45). To determine whether ISGylation could  
193 be involved in DV restriction, we generated HERC5-deficient A549 cells using  
194 CRISPR/Cas9 (Figure S3A) and accordingly, A549 HERC5 null cells were not  
195 able to perform ISGylation after IFN-I treatment (Figure 3A). In contrast to  
196 ISG15 null cells, we did not observe differences between WT and HERC5-  
197 deficient cells when we evaluated both plaque area (Figure 3B) and number  
198 of infected cells per plaque following infection with DV (Figure 3C). Therefore,  
199 ISGylation is not sufficient to inhibit DV replication.

200

201

202

203

204 *ISG15 is necessary for autocrine IFNAR1-mediated control of DV replication*

205

206 ISG15 and its binding partner USP18 are crucial for IFN-I pathway down-  
207 regulation, which is pivotal for infection control and immune-regulation in  
208 humans (28, 29, 46). The A549 ISG15-KO cell line exhibited a lower  
209 expression of USP18 and sustained ISG expression, as exemplified by IFIT3,  
210 after IFN-I stimulation (Figure S4), reproducing the phenotype observed in  
211 cells isolated from humans lacking ISG15 (29).

212 While our single-cell RNA-seq analysis showed that both ISG15 and USP18  
213 are upregulated in PMBCs containing DV RNA, there was an asynchrony of  
214 ISGs being expressed in infected versus bystander cells, with a greater  
215 spectrum present in the latter (Figure 1C). This is expected as flavivirus'  
216 control of IFN-I signaling occurs mainly via its intracellular non-structural  
217 proteins (47, 48) and few ISGs can be directly induced by IRF3 (49–51).

218 Of interest, STAT2 mRNA is expressed at higher levels in DV RNA-containing  
219 cells when compared to bystanders and uninfected cells (Figure 1C). Hence,  
220 we hypothesized that ISG15 interference with DV replication is associated  
221 with autocrine IFN-I signaling in infected cells. Confirming the results from  
222 PMBCs and HuH7 cells, ISG15 mRNA was induced in A549 cells during DV  
223 infection (Figure 4A). As expected, this expression was abolished in knockout  
224 cells. Therefore, we measured the activation of the IFN-I pathway in WT and  
225 ISG15-KO cells infected with DV. Despite ISG15-knockout cells having full  
226 machinery to control viral infection as well as hyper-responsiveness to  
227 exogenous IFN $\alpha$  (Figure S5, Figure 4E and F) (28, 29), they did not respond  
228 properly to DV infection. Infected ISG15-deficient cells had less STAT1  
229 phosphorylation and IFIT1 expression when compared to WT cells and as  
230 expected had no detectable USP18 (Figure 4B). Infected knockout cells  
231 induced IFN $\beta$  mRNA at higher levels than the WT but had less IFIT1 mRNA  
232 (Figures 4C and D) indicating that DV infection impairs the response at both  
233 mRNA and protein levels downstream of IFN-I induction.

234 Taken together, our results suggest that ISG15 inhibits DV infection by  
235 regulating early events of the IFN-I receptor activation. To test this, we

236 constructed an ISG15/IFNAR1 double knockout cell line based on the ISG15-  
237 KO background (Figure S3B). Cells were infected with DV and plaque area  
238 and number of infected cells per plaque was quantified. In parallel, we  
239 performed this experiment in IFNAR1 knockout cells, previously generated by  
240 our group (52, 53). The same phenotype was observed in all three cell lines,  
241 with no additive or synergistic effects in the double knockout (Figures 4G and  
242 H), which places intracellular ISG15 downstream of IFNAR1 signaling in the  
243 control of DV infection.

244

245 *ISG15 counteracts DV IFN-I evasion*

246

247 Flaviviruses are known to counteract IFN-I signaling by inducing the  
248 degradation of STAT2, a key protein in the interferon signal transduction  
249 pathway (11, 14, 54). As our previous results suggest that ISG15's role during  
250 DV infection is downstream of IFNAR engagement (Figure 4), we evaluated  
251 DV-mediated STAT2 degradation in the absence of ISG15. In agreement with  
252 others (55), STAT2 degradation in the A549 cell line occurs rapidly after  
253 infection. Despite showing sustained activation of IFN-I signaling (Figure S4),  
254 ISG15-KO cells showed pronounced STAT2 degradation when infected with  
255 DV (Figure 5A and E-upper panel). As infected IFN-secreting cells are able to  
256 induce an antiviral state in neighboring-bystander cells by inducing the  
257 expression of ISGs (56), we then evaluated in which cell population, infected  
258 and/or bystander, ISG15 impacted DV infection. DV plaques were co-stained  
259 for flavivirus E protein and IFIT3 and confocal microscopy was performed.  
260 Both infected and bystander cells were able to respond to infection, producing  
261 IFIT3 (Figure 5D, top panel). However, IFIT3 expression in the plaque context  
262 was largely impaired and restricted to infected cells in the absence of ISG15  
263 (Figures 5B, C and D). This data suggests that restriction of DV replication  
264 and dissemination is achieved by both autocrine and paracrine IFN-I response  
265 amplification and is dependent on ISG15 expression. To further investigate  
266 this, we sorted DV envelope protein positive and negative cells (Figure S5A  
267 and B), therefore enabling us to evaluate the impact of infection in virus-  
268 containing and bystander cells, respectively. Strikingly, DV-positive cells had  
269 a lower expression of STAT2, IFIT3 and USP18 when compared to bystander

270 cells; a phenotype that was markedly enhanced in ISG15-deficient cells  
271 (Figure 5E, *bottom panel*). While also confirming DV inhibition of IFNAR  
272 signaling, our results further suggest that ISG15 function is targeted for  
273 successful viral infection.

274

275 *USP18 expression overcomes ISG15 deficiency*

276

277 STAT2 degradation mediated by all DV serotypes and ZIKV is largely  
278 dependent on NS5 (11, 14), the virus RdRp and methyltransferase. NS5 was  
279 shown to bind to the N-terminus of human STAT2 (11, 15). Interestingly,  
280 USP18 interacts with STAT2 via its coiled-coil and DNA binding domains. This  
281 causes negative regulation of IFNAR signaling by displacing JAK1 from chain  
282 2 of the receptor (25). As shown here (Figures 4B, 5E and S4) and elsewhere  
283 (28, 29), the absence of ISG15 results in USP18's destabilization. We  
284 therefore examined if NS5 is also present in the STAT2/USP18 complex. In  
285 HEK293 cells lacking ISG15 (Figure S3C, D and E) and primed with IFN $\alpha$  for  
286 18 hours, both endogenous STAT2 and overexpressed USP18, immuno-  
287 precipitated with ZIKV's NS5 (Figure 6A, lane 2). This interaction was  
288 enhanced when a protease-deficient high-expressing USP18 mutant (C64A)  
289 was used (Figure 6A, lane 3). We then hypothesized that the interaction of  
290 USP18 with STAT2 competes with NS5 binding, which in turn could result in a  
291 lower efficiency of virus evasion mechanism. To test this, we performed an  
292 endogenous STAT2 pull-down in ISG15-deficient HEK293 cells transfected  
293 with NS5, USP18 or a combination of both, followed by treatment with IFN $\alpha$   
294 overnight. In the absence of NS5, USP18 interaction with STAT2 was  
295 markedly enhanced (Figure 6B, lanes 2 and 3), suggesting that both proteins  
296 indeed compete for the same region of the protein.

297 Thus, we evaluated whether the presence of USP18 could restore STAT2  
298 expression in ISG15 knockout cells during DV infection. Overexpression of  
299 USP18 led to an increase of STAT2 levels similar to ones seen in wild type  
300 cells (Figure 6C). Importantly, USP18 reconstitution in ISG15-deficient cells  
301 was also able to reduce virus replication (Figure 6D), suggesting that

302 reestablishment of the IFN-I signaling was sufficient to recover the WT  
303 phenotype in ISG15 knockout cells.

304 Together, the results presented here reveal that human ISG15 restricts DV  
305 and ZIKV replication via its ability to stabilize USP18 and regulate the type 1  
306 IFN signaling pathway.

307

## 308 **DISCUSSION**

309

310 A successful infection is dependent on the virus replication machinery and its  
311 ability to evade host immunity. One of the first lines of defense a virus has to  
312 overcome is a plethora of antiviral genes induced by IFN-I (57).

313 ISG15 is induced early during infection (33, 58) and has been shown to have  
314 a viral restriction role in several infection models. Most of those have been  
315 reported to be a consequence of ISGylation (42–44, 59), even though this  
316 process was suggested to be both inefficient and unspecific (59). Here we  
317 show that during the IFN-I response elicited throughout DV infection, direct  
318 viral protein ISGylation is redundant for antiviral immunity; rather, ISG15's  
319 ability to stabilize USP18 prevents NS5-mediated STAT2 degradation, thus  
320 leading to a more effective interferon response that culminates in DV and  
321 ZIKV restriction.

322 Many of ISG15's functions have been shown to be immunomodulatory. For  
323 instance, ISGylation stabilizes IRF3 by occluding its ubiquitylation sites (60),  
324 negatively regulates RIG-I (61) and activates PKR (62). Secreted ISG15  
325 functions as a cytokine (16, 63), leading to the production of IFNy and IL-10 in  
326 human cells, crucial to the control of pathogens such as *Mycobacterium*  
327 *tuberculosis* (17, 19). Moreover, free intracellular ISG15 is essential for  
328 USP18 stability (Figures, 4B, 5E, S4 and (28, 29) and its absence leads to  
329 severe interferonopathy in humans (28). Also there are reports of ISG15  
330 having an antiviral function independent of Ube1L during Chikungunya virus  
331 infection in mice (28, 64), where free ISG15 contributes to infection control by  
332 blunting potentially pathologic levels of cytokine effectors. Considering this  
333 range of functions, it is expected that different pathogens might interact with  
334 this pathway in different ways, according to its co-evolutionary history.

335 Of note, NK, NKT and monocytes were the PBMC populations with higher  
336 upregulation of ISG15 mRNA in single-cell gene expression studies. These  
337 have been shown to be the major producers and/or targets of free  
338 extracellular ISG15 in other contexts (17–19, 63). The influence of  
339 extracellular ISG15 during viral infections should be further explored in the  
340 future.

341 Interestingly, humans lacking ISG15 do not have increased susceptibility to  
342 common viral infections, such as influenza and HSV-1. The explanation for  
343 this, as suggested elsewhere, may lie in the sustained IFN-I response of their  
344 cells creating a hostile environment for virus growth (28, 29). Here, we reveal  
345 that ISG15 restricts DV and ZIKV replication indirectly by stabilizing USP18  
346 and thereby disrupting NS5-STAT2 interaction: ISG15 promotes competition  
347 for a niche exploited by such viruses. We also demonstrate that USP18,  
348 STAT2 and NS5 co-immunoprecipitate, suggesting a very narrow window of  
349 opportunity that NS5 has to degrade STAT2. As USP18/ ISG15 interaction is  
350 reported to down-regulate IFN-I signaling in humans but not mice (29), it is  
351 tempting to speculate that NS5 interaction with STAT2, a major flavivirus  
352 immune evasion mechanism and also restricted to humans (15), was shaped  
353 by the USP18/ISG15 interaction.

354 Our results suggest an unexpected mechanism by which ISG15 can exert an  
355 antiviral function distinct from the debilitating effects of its conjugation to viral  
356 proteins. The key role of IFN-I in viral infections might lead to the perception  
357 of ISGs having a necessarily direct antiviral function, a paradigm that is  
358 recently being reassessed, with a range of ISGs being implicated in infection-  
359 independent functions (65, 66). Here we provide mechanistic insight of the  
360 arms race between ISG15, USP18 and NS5 which suggests that  
361 protein/protein dynamics adjacent to IFNAR are a key determinant for the  
362 outcome of flavivirus infection.

363

#### 364 **ACKNOWLEDGMENTS**

365 This work was supported by Comissão de Aperfeiçoamento de Pessoal de  
366 Nível Superior (CAPES) Computational Biology programme  
367 (23038.010048/2013-27), Conselho Nacional de Desenvolvimento Científico e  
368 Tecnológico (CNPq) (311406/2017-3 and 407609/2018-0) and the Academy

369 of Medical Sciences/U.K. (NAF004/1005) to D.S.M. Howard Hughes Medical  
370 Institute – Early Career Scientist to A.B. (55007412), Wellcome Trust and  
371 Royal Society Sir Henry Dale Fellowship (202471/Z/16/Z) to T.R.S. Wellcome  
372 Trust PhD Studentship (105389/Z/14/Z) to T.J.S. CAPES scholarship  
373 (88887.195782/2018-00) to E.L.R. CNPq scholarship (205096/2018-2) to J.B.  
374 We thank Dr. Sandra Pellegrini and Dr. Carsten Münk for kindly providing  
375 human USP18 plasmids. We thank Dr. Brian Ferguson for critical reading of  
376 the manuscript.

377

### 378 **AUTHOR CONTRIBUTIONS**

379 Conceptualization, C.E.E., A.B. and D.S.M.; Methodology, C.E.E., E.L.R and  
380 D.S.M.; Software, E.L.R; Formal Analysis, C.E.E., E.L.R and E.G.K.,  
381 Investigation, C.E.E., A.A.S., D.O.P, G.M. and JB; Resources, C.E.E., A.A.S,  
382 P.F.S., Z.G, T.J.S., T.F. and T.R.S. Data Curation, E.L.R. and E.G.K., Writing-  
383 Original Draft, C.E.E. and D.S.M., Writing-Review and editing, C.E.E, E.L.R,  
384 D.O.P., E.G.K., P.F.S., J.B., T.J.S., T.F., T.R.S, A.B., and D.S.M.,  
385 Visualization, C.E.E., E.L.R. and D.S.M., Supervision, D.S.M., Project  
386 Administration and Funding Acquisition, D.S.M.

387

### 388 **DECLARATION OF INTERESTS**

389 The authors declare no competing interests.

390

### 391 **FIGURE LEGENDS**

#### 392 **Figure 1. ISG15 is expressed in DV-infected cells**

393 (A) tSNE was used to visualize the single-cell global transcriptome data. Blue  
394 dots represent uninfected cells, derived from healthy donors. Beige dots  
395 represent bystander cells and red dots represent infected cells, both derived  
396 from patients infected with DV.

397 (B) Differential expression of ISGs in PBMCs of patients infected with DV. The  
398 Gene Ontology term “type one interferon” was used to filter the results from  
399 the single-cell RNA sequencing.

400 (C) Single cell ISG expression variability in uninfected, bystander and  
401 infected. ISGylation related genes are underlined. Blue bar represents  
402 uninfected cells, derived from healthy donors. Beige bar represents bystander

403 cells and red bar represents infected cells, both derived from patients infected  
404 with DV.

405 (D) Violin plot representing the expression of ISGylation family members in  
406 uninfected [U], bystander [B] and infected [I] PMBC.

407 (E) Expression of ISG15 in DV infected PMBCs. Size is proportional to the  
408 percentage of infected cells in each cell type. Color intensity represents  
409 ISG15 average expression.

410

411 **Figure 2. ISG15 restricts DV and ZIKV replication**

412 (A) A549 WT and ISG15 KO were infected with 20 DV PFUs. At 36 hpi cells  
413 were fixed, permeabilized and stained for the flavivirus E protein using 4G2  
414 antibody. Displayed images were acquired with a Leica DMI6000 B  
415 microscope.

416 (B and C) DV relative plaque area (B) and the number of infected cells per  
417 plaque (C) quantified by ImageJ software and analyzed using Welch's t test.  
418 Error bars represent mean  $\pm$  SD. Results are representative of three  
419 independent experiments.

420 (D, E and F) Multiple-step DV growth curve in A549 cells. Shown is the  
421 percentage of cells infected as measured by E protein staining (4G2+) (D),  
422 extracellular DV mRNA (PrM) relative expression by RT-qPCR (E) and  
423 titration by focus forming assay (FFA) (F). Statistical analyses were conducted  
424 using unpaired t tests. Error bars represent mean  $\pm$  SD. Results are  
425 representative of three independent experiments.

426 (G) Changes in genomic DV mRNA relative expression over time following  
427 binding of DV to A549 WT and ISG15 KO cells at 4°C and analyzed using  
428 unpaired t test. Error bars represent mean  $\pm$  SD. Results are representative of  
429 two independent experiments.

430 (H and I) Complementation of A549 ISG15 KO cells with ectopically  
431 expressed ISG15. Shown is the percentage of cells infected 36 hpi as  
432 measured by E protein staining (4G2+) (H) and DV mRNA relative expression  
433 by RT-qPCR (I). One-way ANOVA was used to analyze these experiments.  
434 EV: empty vector. Error bars represent mean  $\pm$  SD. Results are  
435 representative of two independent experiments.

436 (J and I) A549 WT and ISG15 KO were infected with 20 ZIKV PFUs. At 36 hpi  
437 cells were fixed, permeabilized and stained for the flavivirus E protein. ZIKV  
438 relative plaque area (J) and number of infected cells per plaque (I), quantified  
439 by ImageJ software and analyzed using unpaired t test with Welch's  
440 correction. Images were acquired with an Olympus IX83 inverted microscope.  
441 Error bars represent mean  $\pm$  SD. Results are representative of three  
442 independent experiments.

443 Statistical analyses were performed using Prism 8 (GraphPad Software). p  
444 values \* $<0.05$ ; \*\* $<0.01$ ; \*\*\* $<0.001$ .

445

446 **Figure 3. ISGylation is not sufficient to restrict DV spread**

447 (A) ISGylation profile of A549 WT and HERC5 KO cells by Western blot. Cells  
448 were primed with IFN $\alpha$ 2b (100 IU/ml) for 24 h and cell lysates were analyzed  
449 with an ISG15 antibody. (\*) indicates antibody unspecific band.

450 (B and C) A549 cells were infected with 20 DV PFUs. At 36 hpi cells were  
451 fixed, permeabilized and stained for the flavivirus E protein. DV relative  
452 plaque area (B) and the number of infected cells per plaque (C) quantified by  
453 ImageJ software and analyzed by one-way ANOVA. Images were acquired  
454 with an Olympus IX83 inverted microscope.

455 Error bars represent mean  $\pm$  SD. Results are representative of three or more  
456 independent experiments. Statistical analyses were performed using Prism 8  
457 (GraphPad Software). p values \*\*\*\* $<0.0001$ .

458

459 **Figure 4. ISG15 is necessary for autocrine IFNAR1-mediated control of  
460 DV replication**

461 (A-D) A549 cells were infected with 20 DV PFU. At 36 hpi, cells were  
462 harvested and the indicated mRNA transcripts were quantified by RT-qPCR  
463 (A, C and D). Cell lysates were analyzed by immunoblotting (B). Error bars  
464 represent mean  $\pm$  SD. Results are representative of two independent  
465 experiments. Data was analyzed by unpaired t test.

466 (E and F) A549 ISG15 KO cells were primed with IFN $\alpha$ 2b (100 IU/ml) for 12 h,  
467 washed three times with DPBS and allowed to rest 12 h before infection with  
468 DV or ZIKV at an MOI of 0.1. Shown is the percentage of cells infected at 36  
469 hpi, as measured by E protein staining (4G2+). Error bars represent mean  $\pm$

470 SD. Results are representative of three independent experiments. Data was  
471 analyzed using unpaired t test.

472 (G and H) A549 cells were infected with 20 DV PFUs. At 36 hpi cells were  
473 fixed, permeabilized and stained for the flavivirus E protein. DV relative  
474 plaque area (E) and number of infected cells per plaque (F) quantified by  
475 ImageJ software and analyzed by one-way ANOVA. Images were acquired  
476 with an Olympus IX83 inverted microscope.

477 Error bars represent mean  $\pm$  SD. Results are representative of three  
478 independent experiments. Statistical analyses were performed using Prism 8  
479 (GraphPad Software). p values \* $<0.05$ ; \*\*\* $<0.001$ .

480

481 **Figure 5. ISG15 counteracts DV IFN-I evasion.**

482 (A) A549 WT and ISG15 KO were infected with 20 DV PFU. Cells were  
483 harvested at the indicated time points after infection (hpi) and cell lysates  
484 were analyzed by Western blot using STAT2 and Actin antibodies.

485 (B, C and D) A549 WT and ISG15 KO immunofluorescence assay (IFA) 36  
486 hpi for cellular IFIT3 and flavivirus E protein expression (D). Percentage of  
487 IFIT3 (B) and DV (C) positive cells per plaque were quantified by ImageJ  
488 software and analyzed using unpaired t test with Welch's correction when  
489 appropriate. Displayed images were acquired with a Leica DMI6000 B  
490 microscope.

491 (E) A549 cells were infected with DV at MOI 0.01. At 36 hpi, cells were fixed,  
492 permeabilized and stained for flavivirus E protein. Cell lysates were analyzed  
493 by Western blot with the indicated antibodies before (upper panel) and after  
494 (bottom panel) cells were sorted by fluorescence-activated cell sorting (FACS)  
495 based on E protein expression.

496 U: uninfected. B: bystander. I: infected.

497 Error bars represent mean  $\pm$  SD. Results are representative of two  
498 independent experiments. Statistical analyses were performed using Prism 8  
499 (GraphPad Software). p values \*\*\* $<0.001$ .

500

501 **Figure 6. USP18 expression overcomes ISG15 deficiency**

502 (A) Flag-tag immunoprecipitation (IP) assay and Western blot analysis of  
503 HEK293 ISG15 KO cells transfected with ZIKV NS5-FLAG, human USP18

504 WT, human USP18 C64A mutant or the empty vector (pcDNA3.1) plasmids,  
505 followed by IFN $\alpha$ 2b (100 IU/ml) priming for 18 h. WCL, whole cell lysate.  
506 Results are representative of three independent experiments.  
507 (B) STAT2 IP assay and Western blot analysis of HEK293 ISG15 KO cells  
508 transfected with the indicated plasmids, followed by IFN $\alpha$ 2b (100 IU/ml)  
509 priming for 18 h. Results are representative of three independent  
510 experiments.  
511 (C and D) Complementation with USP18 in A549 ISG15 KO cells. Cells were  
512 stably transfected with human USP18 or the empty vector and infected with  
513 DV at an MOI of 0.01. At 36 hpi, cells were harvested and cell lysates were  
514 analyzed by Western blot with the corresponding antibodies (C). Percentage  
515 of cells infected as measured by E protein staining (D). Error bars represent  
516 mean  $\pm$  SD. Results are representative of two independent experiments.  
517 Statistical analyses were conducted using Mann-Whitney's test in Prism 8  
518 (GraphPad Software. p value \*\*<0.01 (D). EV: empty vector.  
519

## 520 **LEAD CONTACT AND MATERIAL AVAILABILITY**

521 Further information and requests for resources and reagents should be  
522 directed to and will be fulfilled by the Lead Contact, Daniel Santos Mansur  
523 (daniel.mansur@ufsc.br)

524

## 525 **MATERIAL AND METHODS**

526

### 527 **Cells and viruses**

528 Mammalian cell lines were maintained at 37 °C under the conditions of a  
529 humidified atmosphere and 5% CO<sub>2</sub>. The human alveolar adenocarcinoma-  
530 derived A549 cells, human embryonic kidney HEK293 and the African green  
531 monkey kidney-derived Vero cells were cultured in Dulbecco's modified  
532 Eagle's medium F-12 (DMEM F12) (Gibco) supplemented with 5% fetal  
533 bovine serum (FBS) (Gibco) and streptomycin/penicillin (100 U/ml) (Gibco).  
534 The *Aedes albopictus* mosquito-derived cell line C6/36 was maintained at  
535 28°C in a BOD in Leibovitz's L-15 medium (L-15) (Gibco) supplemented with  
536 10% FBS (Gibco), 0.26% tryptose phosphate broth (Sigma) and 50 µg/ml

537 gentamicin (Sigma). A549 ISG15 KO and IFNAR1-KO have been described  
538 elsewhere (17, 52, 53). All cells were negative for mycoplasma.  
539 Dengue virus serotype 4 (DENV-4 TVP/360 – GenBank accession number:  
540 KU513442) and Zika virus (ZV BR 2015/15261 - GenBank accession number:  
541 MF073358) stocks were propagated in C6/36 cells and titrated in Vero cells.  
542 Vesicular stomatitis virus-green fluorescent protein (VSVeGFP) (Indiana  
543 strain, Marques-JT, Plos Pathogens 2013) and Herpes simplex virus-1-green  
544 fluorescent protein (HSV-1eGFP) (SC16) viruses were propagated and  
545 titrated in Vero cells. HSV-1eGFP was a kind gift of Professor Stacey  
546 Efstathiou.

547

#### 548 **Single-cell RNA sequencing analysis**

549 Processed, publicly available single-cell RNA-seq data are available through  
550 the GEO accession numbers GSE116672 and GSE110496. We downloaded  
551 processed single-cell data and metadata from the supplementary information  
552 from the respective publications (31, 32).

553 Then, we used CellRouter to analyze these datasets. To perform the tSNE  
554 analysis using single-cell data generated by Zanini 2018 (32), we set the  
555 parameters num.pcs=10, seed=1 and max\_iter=1000 in the computeTSNE  
556 function. Next, we identified genes preferentially expressed in Uninfected,  
557 Bystander and Infected cells using a cutoff for the log2 fold change of 0.25.  
558 We used a customized script to obtain all genes containing the keywords  
559 “type I interferon” in the Gene Ontology Biological Processes (package  
560 versions: org.Hs.eg.db\_3.10.0, GO.db\_3.10.0). Next, we took the overlap of  
561 type I interferon genes with the genes preferentially in each condition reported  
562 above. The remaining analyses were focused on these genes.

563 To perform the tSNE analysis using the single-cell data generated by Zanini  
564 2018 (31), we set the parameters num.pcs=20, seed=1 and max\_iter=1000 in  
565 the computeTSNE function. We used a strategy similar to the one described  
566 above to identify genes differentially expressed in each condition but used a  
567 cutoff of 0.15 for this dataset. The parameter num.pcs was determined using  
568 the elbow approach, as described in the CellRouter tutorial at  
569 <https://github.com/edroaldo/cellrouter>.

570

571 **CRISPR/Cas9-mediated gene editing**

572 A549 WT and ISG15 KO cells were co-transfected with two Herc5 or Ifnar1-  
573 targeting gRNA CRISPR/Cas9-GFP plasmids, respectively. HEK293 WT cells  
574 were transfected with three lsg15-targeting gRNA CRISPR/Cas9-GFP  
575 plasmids (Table S1) (Horizon Cambridge, UK). After 72 h, cells were sorted  
576 by FACS (FACSMelody, BD) and single-cell derived clones were initially  
577 screened by PCR genotyping. Additionally, both HERC5 and ISG15/IFNAR1  
578 (dKO) clones were functionally tested by assessing their ISGylation profile  
579 and expression of ISGs, respectively, after IFN $\alpha$  priming. Briefly, A549 WT  
580 and HERC5 and dKO clones were primed with IFN $\alpha$ 2b (100 IU/ml) (PBL  
581 Assay Science) for 24 h and the expression of ISG15-conjugates and IFIT3  
582 was analyzed by Western blot. HEK293 cells were primed with IFN $\alpha$ 2b (1000  
583 IU/ml) for 8 h, total RNA was isolated and lsg15 mRNA expression was  
584 assessed by RT-qPCR.

585

586 **Viral infection**

587 A549 cells were seeded one day prior to infection in appropriate multi-well  
588 plates. For plaque assay, a viral inoculum containing 20 plaque forming units  
589 (PFU) of the corresponding virus was added to each well, and virus  
590 adsorption was performed in DMEM supplemented with  
591 penicillin/streptomycin (100 U/ml) for 90 min at 37°C. Cells were washed with  
592 PBS to remove un-adsorbed virus, and maintained in DMEM 1.5%  
593 carboxymethylcellulose sodium (CMC) (Sigma). Alternatively, cells were  
594 infected with DV at the indicated MOI, as described above, and maintained in  
595 DMEM supplemented with 1% FBS.

596

597 **Titration**

598 DV titration was performed by focus forming assay (FFA) in C6/36 cells.  
599 Briefly, C6/36 cells were seeded ( $1 \times 10^5$  cells/well in 24 well plate) and after  
600 overnight incubation were infected with a 10-fold serial dilution of virus  
601 samples (cell culture supernatants) in L-15 with 0.26% tryptose and 25  $\mu$ g/ml  
602 of gentamicin. After 90 minutes, the inoculum was removed and a CMC  
603 overlay media (L-15 media with 5% FCS, 0.26% tryptose, 25  $\mu$ g/ml of  
604 gentamicin and 1.6% of CMC) was added and the plates were incubated for 7

605 days at 28°C. After incubation, cells were washed, fixed with 3%  
606 paraformaldehyde (PFA) (Sigma-Aldrich) and permeabilized with 0.5% triton  
607 X100 (Sigma-Aldrich). After washing, cells were immunostained with mouse  
608 monoclonal anti flavivirus E protein antibody 4G2 (ATCC® HB-112™, dilution  
609 1:100), followed by goat anti-mouse immunoglobulin conjugated to alkaline  
610 phosphatase (Promega S3721, dilution 1:7500). Focuses of infection were  
611 revealed using NBT/BCIP reagent (Promega), following the manufacturer's  
612 instructions and the virus titer calculated as follow: media of focus  
613 number/inoculum volume x dilution. The results are expressed as FFU<sub>C6/36</sub>/ml  
614 (Gould et al., 1985).

615 VSVeGFP and HSV-1eGFP titrations were performed by plaque assay.  
616 Briefly, Vero cells were seeded in 24-well plates 24 h prior to infection. Cell  
617 monolayers were washed with PBS and inoculated with 0.3 ml of serial 10-  
618 fold dilutions of the virus in duplicates. After 90 min adsorption at 37°C, each  
619 well was re-suspended in DMEM 1.5% CMC. At 48 hpi, cells were fixed with  
620 3% PFA (Sigma) for 30 min, washed 3 times with PBS and stained with 1%  
621 crystal violet (Sigma) for 30 min at room temperature. Virus yield was  
622 calculated and expressed as plaque forming units per ml (PFU/ml).

623

## 624 **Immunofluorescence**

625 At 24 hpi and 18 hpi, respectively, HSVeGFP and VSVeGFP infected cells  
626 were fixed with 3% PFA for 20 min at room temperature, permeabilized with  
627 0.5% Triton X100 in PBS for 4 min and stained with DAPI counterstain  
628 (Molecular Probes). At 36 hpi, DV and ZIKV infected cells were fixed,  
629 permeabilized and stained with mouse monoclonal 4G2 antibody (10 µg/ml  
630 dilution 1:100), followed by incubation with Alexa Fluor 488 rabbit anti-mouse  
631 IgG (H<sub>2</sub>+L, Life Technologies, dilution 1:500), and DAPI counterstain.  
632 Images were acquired with an Olympus IX83 inverted microscope. Briefly,  
633 virus plaques, determined by eGFP or flavivirus E protein expression, were  
634 delimited; images were converted to 16-bit and processed to be analyzed with  
635 the ImageJ Software Cell Counter Plugin (W. S. Rasband, ImageJ, US  
636 National Institutes of Health, Bethesda, MD; <http://rsb.info.nih.gov/ij/>, 1997–  
637 2006).

638 For confocal analysis, A549 cells grown on glass coverslips were mock  
639 infected or infected with 10 DV PFU. At 36 hpi, cells were fixed and  
640 permeabilized. Following washes with PBS, cells were stained with mouse  
641 monoclonal anti-E protein (4G2, dilution 1:100) and rabbit polyclonal anti-  
642 IFIT3 (Proteintech, 15201-1-AP, dilution 1:200) for 1 h at room temperature.  
643 The cells were washed with PBS and stained with secondary antibodies Alexa  
644 Fluor 488 goat anti-mouse IgG (H<sub>+</sub>L, Life Technologies, dilution 1:500) and  
645 Alexa 568 goat anti-rabbit IgG (H+L, Life Technologies, dilution 1:500) and  
646 DAPI counterstain (Molecular Probes). Cells were washed and coverslips  
647 mounted using Prolong antifade reagent (Invitrogen). Z-stack and max  
648 intensity projection images were generated with a Leica DMI6000 B confocal  
649 microscope and Leica Application Suite X software for image analysis (Leica  
650 Microsystems).

651

## 652 **Flow cytometry and cell sorting**

653 Cells were fixed with 2% PFA in PBS, washed twice with PBS and  
654 permeabilized with 0.5% saponin in 1% BSA in PBS. Anti-flavivirus E protein  
655 mAb 4G2 was conjugated to Alexa Fluor 488 5-SDP (Life Technologies)  
656 following the manufacturer's instructions. Cells were incubated with FITC-  
657 conjugated 4G2 (dilution 1:1000) in permeabilization buffer for 40 minutes at  
658 room temperature, washed once and resuspended in FACS buffer. The cell  
659 suspensions were analyzed by flow cytometry on a FACSVerse instrument  
660 (BD Biosciences) and analyzed using FlowJo V10 software (BD). Cell sorting  
661 experiments were performed on a FACSMelody cell sorter (BD Biosciences).

662

## 663 **RT-qPCR**

664 vRNA was isolated by using QIAamp viral RNA Mini Kit (Qiagen). Intracellular  
665 total RNA was isolated with TRIZOL (Thermo Life) following manufacturer's  
666 instructions. A total of 1 µg was reverse transcribed using the High capacity  
667 cDNA reverse transcription kit (Applied Biosystems). Quantitative PCRs  
668 (qPCRs) were performed with GoTaq ® qPCR Master mix (Promega) using  
669 StepOne Plus real time PCR system (Applied Biosystems). VSVeGFP and  
670 18S mRNA were used as control housekeeping genes. Amounts of DV or ISG

671 mRNA were calculated by using the  $\Delta\Delta CT$  method. Primers specific the  
672 mRNA analyzed are listed in Table S1.

673

674 **Western blot**

675 Human antibodies used for immunoblot were as follows: mouse mAb to  $\beta$ -  
676 actin (Abcam, ab6276, dilution 1:4000), rabbit mAb to IFIT1 (Abcam,  
677 ab137632, dilution 1:1000), mouse mAb to pSTAT1(Y701) [M135] (Abcam,  
678 ab29045, dilution 1:1000), mouse mAb to STAT1 (Abcam, ab3987, dilution  
679 1:1000), rabbit pAb to IFIT3 (ProteinTech, 15201-1-AP, dilution 1:1000), rabbit  
680 mAb to USP18 [D4E7] (Cell Signaling Technologies, 4813, dilution 1:1000),  
681 rabbit mAb to STAT2 [D9J7L] (Cell Signaling Technologies, 72604, dilution  
682 1:1000), mouse mAb to ISG15 (R&D System, MAB4845, dilution 1:1000),  
683 home-made mouse mAb anti-GFP (67, 68) (dilution 1:1000) and mouse mAb  
684 to FLAG tag (Sigma, F3165, dilution 1:500).

685 Cells were treated as indicated, wash two times with ice-cold PBS and then  
686 lysed in RIPA buffer [50 mM tris-HCl (pH 7.5), 150 mM NaCl, 1% Triton X100,  
687 0.5% sodium deoxycholate, 0.1% SDS, 5 mM EDTA] supplemented with 1x  
688 protease inhibitors (Mini Protease Inhibitor Tablets, Roche). Total protein  
689 concentration was determined by BSA Protein Assay Kit (Thermo Life). For  
690 western blotting, 20  $\mu$ g of total protein were prepared in dithiothreitol-  
691 containing Laemmli sample buffer, separated and transferred to a  
692 nitrocellulose blotting membrane (GE Healthcare Amersham). After transfer,  
693 the membrane was blocked with 5% nonfat dry milk in TBS 0.1% Tween 20  
694 (TBST) for 1 h at room temperature. Membrane was incubated with primary  
695 Abs diluted in 2% BSA in TBST at 4°C with gentle shaking overnight.  
696 Membrane was washed three times with TBST and then incubated with the  
697 appropriate secondary HRP-linked antibody for 1 h at room temperature.  
698 Membranes were washed and covered with ECL developing solution  
699 (Pierce™ ECL WB substrate, Thermo Fisher Scientific).

700

701 **Plasmids and transfections**

702 Herc5 and Ifnar1 sgRNA/Cas9/GFP plasmids were provided by Horizon  
703 (Cambridge, UK). sgRNA sequences are described in Supplementary Table  
704 1. Expression plasmid for ISG15 was described elsewhere (17). Pmax™ GFP

705 expression vector was acquired from Lonza (cat numb #D-00061). Expression  
706 plasmid for ZIKV NS5 was generated by amplifying the NS5 coding sequence  
707 (amino acids 2521-3423 in the polyprotein) from a previously described  
708 plasmid-based ZIKV reverse genetic system (69) using primers containing an  
709 N-terminal FLAG tag and inserted into pcDNA3.1. Expression plasmids for  
710 human USP18 WT and USP18 C64A mutant were kindly provided by Dr  
711 Carsten Münk (70). Transfections were performed with FuGene6 (Promega),  
712 following the manufacturer's instructions. Stably transfected cells were  
713 selected with geneticin (500 µg/ml) (Sigma).

714

### 715 **Immunoprecipitation**

716 For Stat2 co-immunoprecipitation assays, cells were lysed in RIPA buffer  
717 composed of 20 mM Tris-HCl pH 7.4, 150 mM NaCl, 10 mM CaCl<sub>2</sub>, 0.1% v/v  
718 Triton X-100, 10% v/v glycerol and complete protease inhibitor cocktail (Mini  
719 Protease Inhibitor Tablets, Roche). The supernatant was separated by  
720 centrifugation at 12.000 g at 4 °C for 10 min and incubated with STAT2  
721 antibody (2 µg) (Santa Cruz Biotechnology, 514193) for 3 h at 4°C with gentle  
722 shaking. Complexes were precipitated with protein A/G Plus-agarose (Santa  
723 Cruz Biotechnology), washed with TBS and resuspended in SDS sample  
724 buffer. Immunoprecipitates were subjected to SDS-PAGE and western  
725 blotting, as described above.

726 FLAG-tagged proteins were immunoprecipitated with anti-FLAG M2-agarose  
727 (Sigma), following the manufacturer's instructions.

728 All assays were performed three times and representative blots are  
729 presented.

730

### 731 **QUANTIFICATION AND STATISTICAL ANALYSIS**

732 Details concerning the statistical analysis methods are provided in each figure  
733 legend. Briefly, all data were analyzed using GraphPad Prism 8 software and  
734 were shown as mean and the standard deviation (SD). Statistical significance  
735 was determined by Welch's t test or one-way ANOVA for plaque size  
736 analyses, unpaired t test for virus multiple-step growth curve, cellular mRNA  
737 quantification and percentage of cells infected. Statistical significance is  
738 indicated by \*, p < 0.05; \*\*, p < 0.01; \*\*\*, p < 0.001.

739

740 **SUPPLEMENTAL INFORMATION**

741

742 **Figure S1**

743 (A) tSNE was used to visualize the single-cell global transcriptome data. Blue  
744 dots represent uninfected cells, derived from healthy donors. Beige dots  
745 represent bystander cells and red dots represent infected cells, both derived  
746 from patients infected with DV.

747 (B) Differential expression of ISGs in HuH7 cells infected with DV. The Gene  
748 Ontology term “type one interferon” was used to filter the results from the  
749 single-cell RNA sequencing.

750 (C) Single cell ISG expression variability in uninfected, bystander and  
751 infected. ISGylation related genes are underlined. Blue bar represents  
752 uninfected cells. Beige bar represents bystander cells and red bar represents  
753 infected cells, both derived from cells exposed to DV.

754 (D) Violin plot representing the expression of ISGylation family members in  
755 uninfected [U], bystander [B] and infected [I] HuH7 cell line.

756

757

758 **Figure S2. ISG15 does not restrict HSV-1 and VSV spread**

759 (A and B) A549 cells were infected with 20 HSV-1eGFP PFU. At 24 hpi, cells  
760 were fixed and stained with DAPI counterstain. HSV-1eGFP relative plaque  
761 area (A) and number of cells per plaque (B). Images were acquired with an  
762 Olympus IX83 inverted microscope and quantified by ImageJ software.

763 (C and D) A549 cells were infected with 20 VSVeGFP PFU. At 18 hpi, cells  
764 were fixed and stained with DAPI counterstain. VSVeGFP relative plaque  
765 area (C) and number of cells per plaque (D). Images were acquired with an  
766 Olympus IX83 inverted microscope and quantified by ImageJ software.

767 Error bars represent mean  $\pm$  SD. Results are representative of three or more  
768 independent experiments. Statistical analyses were conducted using Mann-  
769 Whitney's test in Prism 8 (GraphPad Software).

770

771 **Figure S3. Characterization of knockout cell lines**

772 (A) Agarose gel electrophoresis of A549 WT and HERC5 KO PCR products  
773 using primers surrounding CRISPR/Cas9 ISG15 sgRNA guides editing region.  
774 PCR product size: WT: 310 bp; HERC5 KO: ~250 bp. (\*) indicates PCR  
775 unspecific band. WT: A549 WT cell line; KO: A549 HERC5 KO; B: blank  
776 (B) Clonal isolates of A549 cells were immunoblotted for IFIT3 after 24 h  
777 treatment with IFN $\alpha$ 2b (100 IU/ml) (+, control IFIT3 -proficient cells; 1–9,  
778 different clonal isolates after limiting dilution).  
779 (C) Agarose gel electrophoresis of HEK293 WT and ISG15 KO PCR products  
780 using primers surrounding CRISPR/Cas9 ISG15 sgRNA guides editing region.  
781 PCR product size: WT: 1016bp; ISG15 KO: ~180bp. (\*) indicates PCR  
782 unspecific band. WT: HEK293 WT cell line; KO: HEK293 ISG15 KO; B: blank  
783 (D) HEK293 WT and ISG15 KO cells were stimulated with IFN $\alpha$ 2b (1000  
784 IU/ml) for 8 h. Cells were harvested and total RNA was isolated. lsg15 mRNA  
785 was analyzed by RT-qPCR.  
786 (E) HEK293 ISG15KO PCR product was cloned into pGEM vector and  
787 sequenced by Sanger method. Nucleotide sequence was aligned with lsg15  
788 reference sequence retrieved from GenBank (NM\_005101) and translated  
789 into primary amino acid sequence. (.) indicates the same sequence; (-) gap;  
790 (\*) stop codon.

791

792 **Figure S4. A549 ISG15 KO cell line exhibits sustained ISG expression**

793 (A) A549 cells were primed with IFN $\alpha$ 2b (100 IU/ml) for 12 h, washed three  
794 times with DPBS and allowed to rest. Cells were harvested at the indicated  
795 time point and cell lysates were analyzed by Western blot with the  
796 corresponding antibodies.

797 Results are representative of two independent experiments.

798

799 **Figure S5. Sorting of infected cells**

800 (A and B) A549 cells were infected with DV at MOI 0.01.  
801 Representative FACS profile and DV mRNA qPCR of WT (A) and ISG15-KO  
802 (B) cells sorted by flavivirus E protein expression (4G2, FITC-A axis).  
803 B: bystander. I: infected

804

805 **REFERENCES**

- 806 1. D. S. Mansur, G. L. Smith, B. J. Ferguson, Intracellular sensing of viral DNA by  
807 the innate immune system. *Microbes Infect.* **16**, 1002–1012 (2014).
- 808 2. A. Gebhardt, B. T. Laudenbach, A. Pichlmair, Discrimination of Self and Non-  
809 Self Ribonucleic Acids. *J. Interferon Cytokine Res.* **37**, 184–197 (2017).
- 810 3. J. W. Schoggins, Interferon-Stimulated Genes: What Do They All Do? *Annu Rev*  
811 *Virol* (2019) <https://doi.org/10.1146/annurev-virology-092818-015756>.
- 812 4. A. García-Sastre, Ten Strategies of Interferon Evasion by Viruses. *Cell Host*  
813 *Microbe* **22**, 176–184 (2017).
- 814 5. T. C. Pierson, M. S. Diamond, The emergence of Zika virus and its new clinical  
815 syndromes. *Nature* **560**, 573–581 (2018).
- 816 6. A. D. T. Barrett, The reemergence of yellow fever. *Science* **361**, 847–848  
817 (2018).
- 818 7. S. Bhatt, *et al.*, The global distribution and burden of dengue. *Nature* **496**, 504–  
819 507 (2013).
- 820 8. D. S. Shepard, E. A. Undurraga, Y. A. Halasa, J. D. Stanaway, The global  
821 economic burden of dengue: a systematic analysis. *Lancet Infect. Dis.* **16**, 935–  
822 941 (2016).
- 823 9. L. Miorin, A. M. Maestre, A. Fernandez-Sesma, A. García-Sastre, Antagonism of  
824 type I interferon by flaviviruses. *Biochem. Biophys. Res. Commun.* **492**, 587–596  
825 (2017).
- 826 10. A. E. Ngono, S. Shresta, Immune Response to Dengue and Zika. *Annu. Rev.*  
827 *Immunol.* **36**, 279–308 (2018).
- 828 11. A. Grant, *et al.*, Zika Virus Targets Human STAT2 to Inhibit Type I Interferon  
829 Signaling. *Cell Host Microbe* **19**, 882–890 (2016).
- 830 12. M. Laurent-Rolle, *et al.*, The interferon signaling antagonist function of yellow  
831 fever virus NS5 protein is activated by type I interferon. *Cell Host Microbe* **16**,  
832 314–327 (2014).
- 833 13. S. Chen, Z. Wu, M. Wang, A. Cheng, Innate Immune Evasion Mediated by  
834 Flaviviridae Non-Structural Proteins. *Viruses* **9** (2017).
- 835 14. J. Morrison, *et al.*, Dengue virus co-opts UBR4 to degrade STAT2 and  
836 antagonize type I interferon signaling. *PLoS Pathog.* **9**, e1003265 (2013).
- 837 15. J. Ashour, *et al.*, Mouse STAT2 restricts early dengue virus replication. *Cell Host*  
838 *Microbe* **8**, 410–421 (2010).
- 839 16. P. F. Dos Santos, D. S. Mansur, Beyond ISGylation: Functions of Free  
840 Intracellular and Extracellular ISG15. *J. Interferon Cytokine Res.* **37**, 246–253  
841 (2017).
- 842 17. P. F. Dos Santos, *et al.*, ISG15-Induced IL-10 Is a Novel Anti-Inflammatory  
843 Myeloid Axis Disrupted during Active Tuberculosis. *J. Immunol.* **200**, 1434–1442  
844 (2018).
- 845 18. C. D. Swaim, A. F. Scott, L. A. Canadeo, J. M. Huibregtse, Extracellular ISG15

- 846        Signals Cytokine Secretion through the LFA-1 Integrin Receptor. *Mol. Cell* **68**,  
847        581–590.e5 (2017).
- 848        19. D. Bogunovic, *et al.*, Mycobacterial disease and impaired IFN- $\gamma$  immunity in  
849        humans with inherited ISG15 deficiency. *Science* **337**, 1684–1688 (2012).
- 850        20. M. Delgobo, *et al.*, An evolutionary recent IFN-IL-6-CEBP axis is linked to  
851        monocyte expansion and tuberculosis severity in humans  
852        <https://doi.org/10.1101/514943>.
- 853        21. B. Skaug, Z. J. Chen, Emerging role of ISG15 in antiviral immunity. *Cell* **143**,  
854        187–190 (2010).
- 855        22. A. Dastur, S. Beaudenon, M. Kelley, R. M. Krug, J. M. Huibregtse, Herc5, an  
856        interferon-induced HECT E3 enzyme, is required for conjugation of ISG15 in  
857        human cells. *J. Biol. Chem.* **281**, 4334–4338 (2006).
- 858        23. J. J. Y. Wong, Y. F. Pung, N. S.-K. Sze, K.-C. Chin, HERC5 is an IFN-induced  
859        HECT-type E3 protein ligase that mediates type I IFN-induced ISGylation of  
860        protein targets. *Proc. Natl. Acad. Sci. U. S. A.* **103**, 10735–10740 (2006).
- 861        24. Y.-C. Perng, D. J. Lenschow, ISG15 in antiviral immunity and beyond. *Nat. Rev.  
862        Microbiol.* **16**, 423–439 (2018).
- 863        25. K.-I. Arimoto, *et al.*, STAT2 is an essential adaptor in USP18-mediated  
864        suppression of type I interferon signaling. *Nat. Struct. Mol. Biol.* **24**, 279–289  
865        (2017).
- 866        26. M. P. Malakhov, O. A. Malakhova, K. I. Kim, K. J. Ritchie, D.-E. Zhang, UBP43  
867        (USP18) specifically removes ISG15 from conjugated proteins. *J. Biol. Chem.*  
868        **277**, 9976–9981 (2002).
- 869        27. O. Malakhova, M. Malakhov, C. Hetherington, D.-E. Zhang, Lipopolysaccharide  
870        activates the expression of ISG15-specific protease UBP43 via interferon  
871        regulatory factor 3. *J. Biol. Chem.* **277**, 14703–14711 (2002).
- 872        28. X. Zhang, *et al.*, Human intracellular ISG15 prevents interferon- $\alpha/\beta$  over-  
873        amplification and auto-inflammation. *Nature* **517**, 89–93 (2015).
- 874        29. S. D. Speer, *et al.*, ISG15 deficiency and increased viral resistance in humans  
875        but not mice. *Nat. Commun.* **7**, 11496 (2016).
- 876        30. D. J. Lenschow, *et al.*, IFN-stimulated gene 15 functions as a critical antiviral  
877        molecule against influenza, herpes, and Sindbis viruses. *Proc. Natl. Acad. Sci.  
878        U. S. A.* **104**, 1371–1376 (2007).
- 879        31. F. Zanini, S.-Y. Pu, E. Bekerman, S. Einav, S. R. Quake, Single-cell  
880        transcriptional dynamics of flavivirus infection. *Elife* **7** (2018).
- 881        32. F. Zanini, *et al.*, Virus-inclusive single-cell RNA sequencing reveals the  
882        molecular signature of progression to severe dengue. *Proc. Natl. Acad. Sci. U.  
883        S. A.* **115**, E12363–E12369 (2018).
- 884        33. I. Ramos, *et al.*, Innate immune response to influenza virus at single-cell  
885        resolution in human epithelial cells revealed paracrine induction of interferon  
886        lambda 1. *J. Virol.* (2019) <https://doi.org/10.1128/JVI.00559-19>.

- 887 34. P. Keskinen, *et al.*, Impaired antiviral response in human hepatoma cells.  
888 *Virology* **263**, 364–375 (1999).
- 889 35. B. Schmid, *et al.*, Live Cell Analysis and Mathematical Modeling Identify  
890 Determinants of Attenuation of Dengue Virus 2'-O-Methylation Mutant. *PLoS*  
891 *Pathog.* **11**, e1005345 (2015).
- 892 36. H. Roth, *et al.*, Flavivirus Infection Uncouples Translation Suppression from  
893 Cellular Stress Responses. *MBio* **8** (2017).
- 894 37. K. Wang, *et al.*, Interferon-stimulated TRIM69 interrupts dengue virus replication  
895 by ubiquitinating viral nonstructural protein 3. *PLoS Pathog.* **14**, e1007287  
896 (2018).
- 897 38. J. N. Whelan, Y. Li, R. H. Silverman, S. R. Weiss, Zika Virus Production Is  
898 Resistant to RNase L Antiviral Activity. *J. Virol.* **93** (2019).
- 899 39. R. C. Gullberg, *et al.*, Stearoly-CoA desaturase 1 differentiates early and  
900 advanced dengue virus infections and determines virus particle infectivity. *PLoS*  
901 *Pathog.* **14**, e1007261 (2018).
- 902 40. J. Zhang, *et al.*, Flaviviruses Exploit the Lipid Droplet Protein AUP1 to Trigger  
903 Lipophagy and Drive Virus Production. *Cell Host Microbe* **23**, 819–831.e5  
904 (2018).
- 905 41. C. Zhao, C. Denison, J. M. Huibregtse, S. Gygi, R. M. Krug, Human ISG15  
906 conjugation targets both IFN-induced and constitutively expressed proteins  
907 functioning in diverse cellular pathways. *Proc. Natl. Acad. Sci. U. S. A.* **102**,  
908 10200–10205 (2005).
- 909 42. C. Zhao, T.-Y. Hsiang, R.-L. Kuo, R. M. Krug, ISG15 conjugation system targets  
910 the viral NS1 protein in influenza A virus-infected cells. *Proc. Natl. Acad. Sci. U.*  
911 *S. A.* **107**, 2253–2258 (2010).
- 912 43. Y. J. Kim, *et al.*, Consecutive Inhibition of ISG15 Expression and ISGylation by  
913 Cytomegalovirus Regulators. *PLoS Pathog.* **12**, e1005850 (2016).
- 914 44. R. González-Sanz, *et al.*, ISG15 Is Upregulated in Respiratory Syncytial Virus  
915 Infection and Reduces Virus Growth through Protein ISGylation. *J. Virol.* **90**,  
916 3428–3438 (2016).
- 917 45. T. Hishiki, *et al.*, Interferon-mediated ISG15 conjugation restricts dengue virus 2  
918 replication. *Biochem. Biophys. Res. Commun.* **448**, 95–100 (2014).
- 919 46. V. François-Newton, *et al.*, USP18-based negative feedback control is induced  
920 by type I and type III interferons and specifically inactivates interferon  $\alpha$   
921 response. *PLoS One* **6**, e22200 (2011).
- 922 47. N. A. Dalrymple, V. Cimica, E. R. Mackow, Dengue Virus NS Proteins Inhibit  
923 RIG-I/MAVS Signaling by Blocking TBK1/IRF3 Phosphorylation: Dengue Virus  
924 Serotype 1 NS4A Is a Unique Interferon-Regulating Virulence Determinant.  
925 *MBio* **6**, e00553–15 (2015).
- 926 48. J. L. Muñoz-Jordán, *et al.*, Inhibition of alpha/beta interferon signaling by the  
927 NS4B protein of flaviviruses. *J. Virol.* **79**, 8004–8013 (2005).
- 928 49. C. Daly, N. C. Reich, Double-stranded RNA activates novel factors that bind to

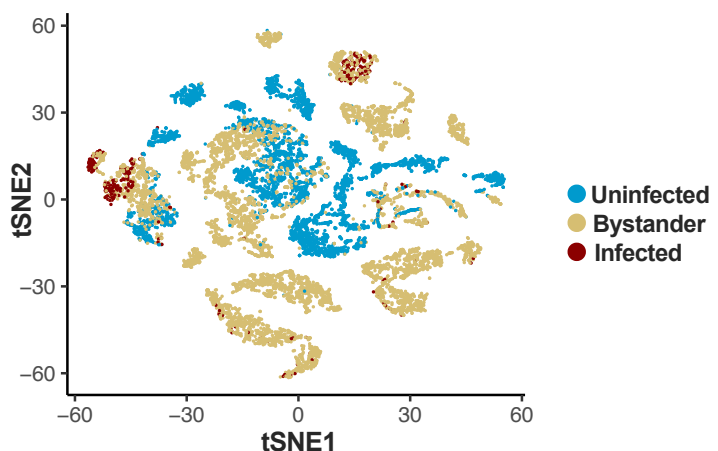
- 929        the interferon-stimulated response element. *Mol. Cell. Biol.* **13**, 3756–3764  
930        (1993).
- 931        50. C. Daly, N. C. Reich, Characterization of specific DNA-binding factors activated  
932        by double-stranded RNA as positive regulators of interferon alpha/beta-  
933        stimulated genes. *J. Biol. Chem.* **270**, 23739–23746 (1995).
- 934        51. B. K. Weaver, K. P. Kumar, N. C. Reich, Interferon regulatory factor 3 and  
935        CREB-binding protein/p300 are subunits of double-stranded RNA-activated  
936        transcription factor DRAF1. *Mol. Cell. Biol.* **18**, 1359–1368 (1998).
- 937        52. E. S. Guimarães, *et al.*, Cyclic Dinucleotides Trigger STING-Dependent  
938        Unfolded Protein Response That Favors Bacterial Replication. *J. Immunol.* **202**,  
939        2671–2681 (2019).
- 940        53. K. H. Antunes, *et al.*, Microbiota-derived acetate protects against respiratory  
941        syncytial virus infection through a GPR43-type 1 interferon response. *Nat.*  
942        *Commun.* **10**, 3273 (2019).
- 943        54. J. Ashour, M. Laurent-Rolle, P.-Y. Shi, A. García-Sastre, NS5 of dengue virus  
944        mediates STAT2 binding and degradation. *J. Virol.* **83**, 5408–5418 (2009).
- 945        55. M. Jones, *et al.*, Dengue virus inhibits alpha interferon signaling by reducing  
946        STAT2 expression. *J. Virol.* **79**, 5414–5420 (2005).
- 947        56. U. Rand, *et al.*, Multi-layered stochasticity and paracrine signal propagation  
948        shape the type-I interferon response. *Mol. Syst. Biol.* **8**, 584 (2012).
- 949        57. W. M. Schneider, M. D. Chevillotte, C. M. Rice, Interferon-stimulated genes: a  
950        complex web of host defenses. *Annu. Rev. Immunol.* **32**, 513–545 (2014).
- 951        58. K. R. Loeb, A. L. Haas, The interferon-inducible 15-kDa ubiquitin homolog  
952        conjugates to intracellular proteins. *J. Biol. Chem.* **267**, 7806–7813 (1992).
- 953        59. L. A. Durfee, N. Lyon, K. Seo, J. M. Huibregtse, The ISG15 conjugation system  
954        broadly targets newly synthesized proteins: implications for the antiviral function  
955        of ISG15. *Mol. Cell* **38**, 722–732 (2010).
- 956        60. H.-X. Shi, *et al.*, Positive regulation of interferon regulatory factor 3 activation by  
957        Herc5 via ISG15 modification. *Mol. Cell. Biol.* **30**, 2424–2436 (2010).
- 958        61. M.-J. Kim, S.-Y. Hwang, T. Imaizumi, J.-Y. Yoo, Negative feedback regulation of  
959        RIG-I-mediated antiviral signaling by interferon-induced ISG15 conjugation. *J.*  
960        *Virol.* **82**, 1474–1483 (2008).
- 961        62. F. Okumura, *et al.*, Activation of double-stranded RNA-activated protein kinase  
962        (PKR) by interferon-stimulated gene 15 (ISG15) modification down-regulates  
963        protein translation. *J. Biol. Chem.* **288**, 2839–2847 (2013).
- 964        63. J. D'Cunha, E. Knight Jr, A. L. Haas, R. L. Truitt, E. C. Borden,  
965        Immunoregulatory properties of ISG15, an interferon-induced cytokine. *Proc.*  
966        *Natl. Acad. Sci. U. S. A.* **93**, 211–215 (1996).
- 967        64. S. W. Werneke, *et al.*, ISG15 is critical in the control of Chikungunya virus  
968        infection independent of UbE1L mediated conjugation. *PLoS Pathog.* **7**,  
969        e1002322 (2011).

- 970     65. F. Vuillier, Z. Li, P.-H. Commere, L. T. Dynesen, S. Pellegrini, USP18 and ISG15  
971       coordinately impact on SKP2 and cell cycle progression. *Sci. Rep.* **9**, 4066  
972       (2019).
- 973     66. S. Dabo, *et al.*, Inhibition of the inflammatory response to stress by targeting  
974       interaction between PKR and its cellular activator PACT. *Sci. Rep.* **7**, 16129  
975       (2017).
- 976     67. C. Zanluca, G. A. C. A. Mazzarotto, J. Bordignon, C. N. Duarte Dos Santos,  
977       Development, characterization and application of monoclonal antibodies against  
978       Brazilian Dengue virus isolates. *PLoS One* **9**, e110620 (2014).
- 979     68. G. F. Silveira, *et al.*, Human T Lymphocytes Are Permissive for Dengue Virus  
980       Replication. *J. Virol.* **92** (2018).
- 981     69. M. Mutso, *et al.*, Reverse genetic system, genetically stable reporter viruses and  
982       packaged subgenomic replicon based on a Brazilian Zika virus isolate. *J. Gen.*  
983       *Virol.* **98**, 2712–2724 (2017).
- 984     70. E. Osei Kuffour, *et al.*, USP18 (UBP43) Abrogates p21-Mediated Inhibition of  
985       HIV-1. *J. Virol.* **92** (2018).

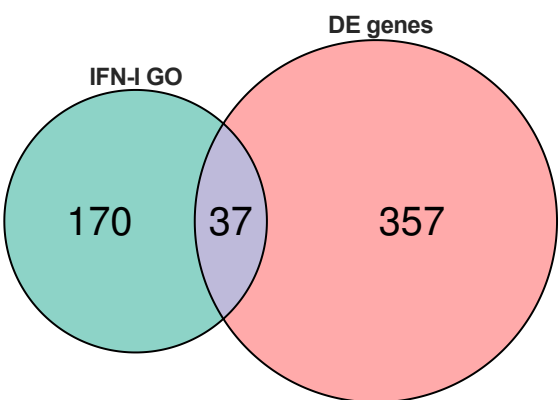
986

**Figure 1-Espada et al.**

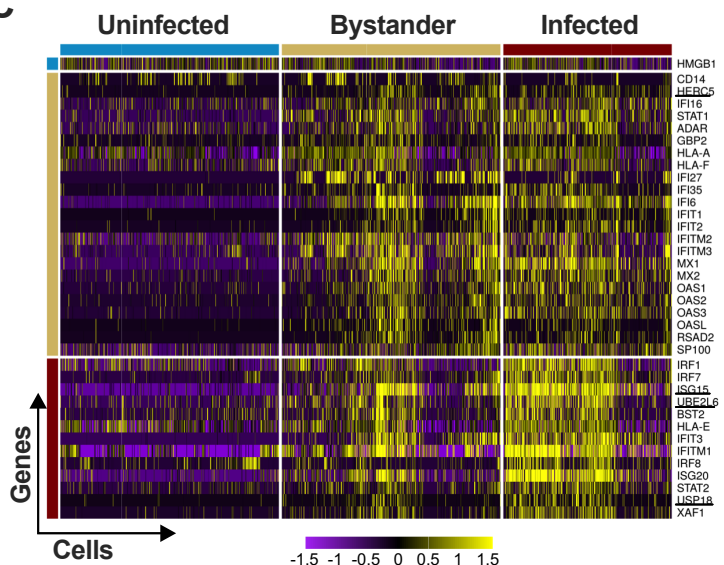
**A**



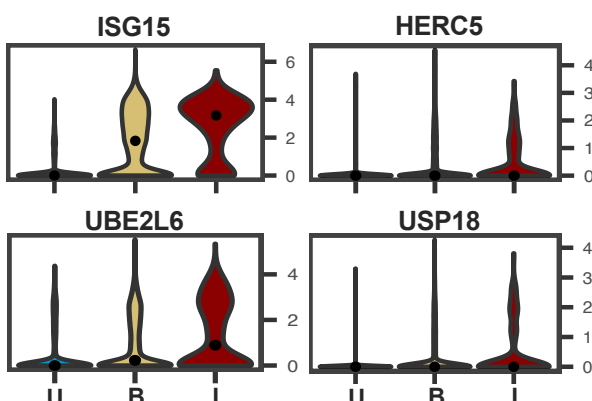
**B**



**C**



**D**



**E**

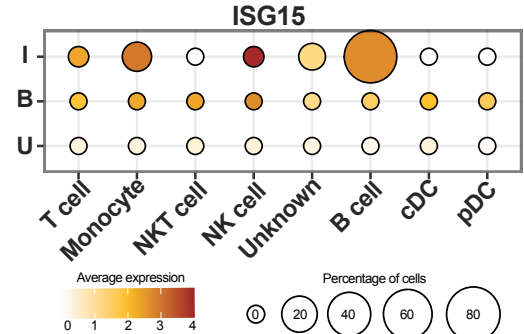


**Figure 2-Espada et al.**

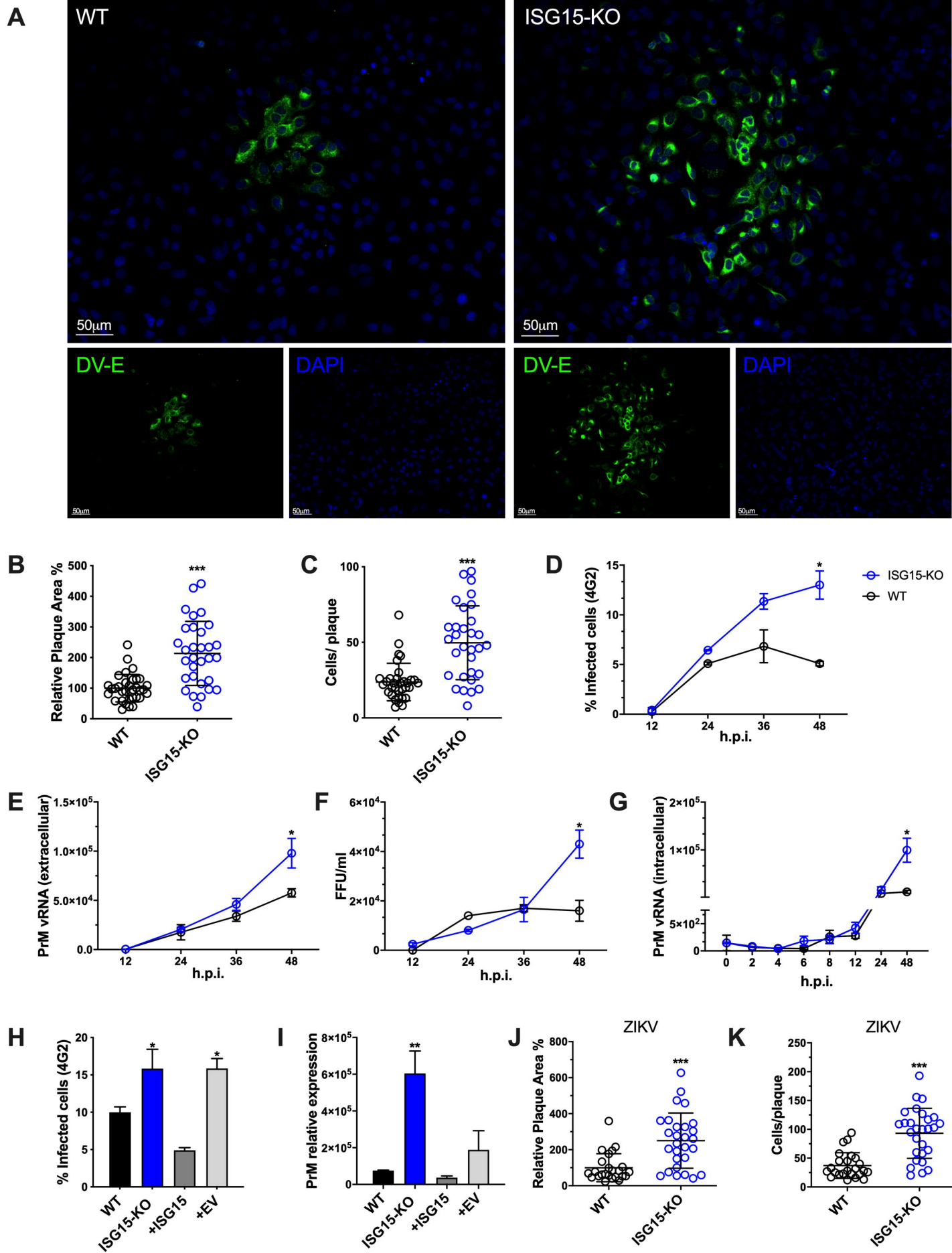


**Figure 3-Espada et al.**

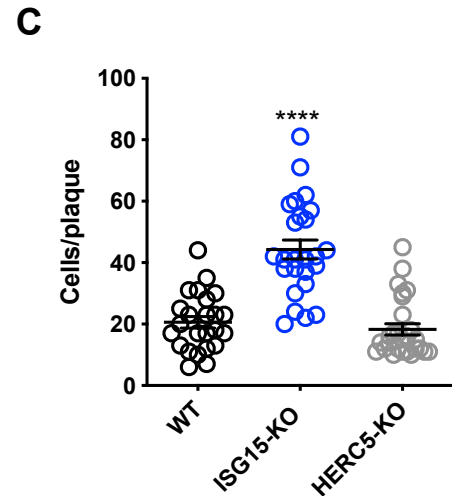
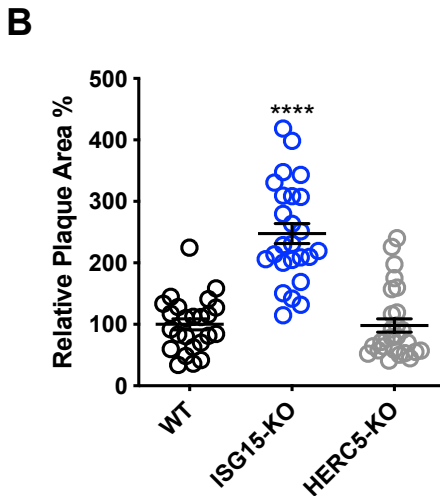
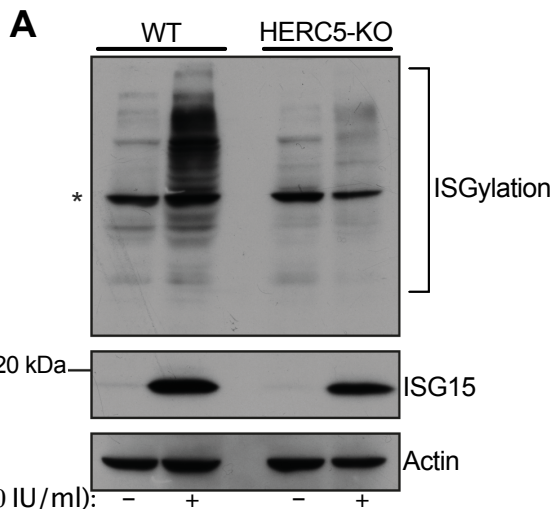
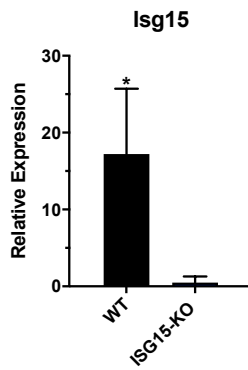
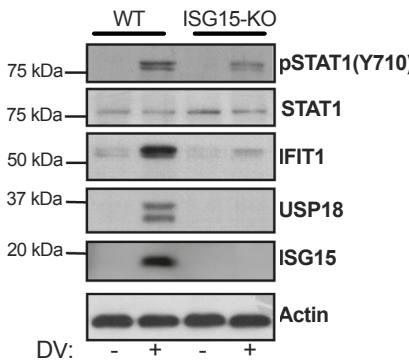


**Figure 4-Espada et al.**

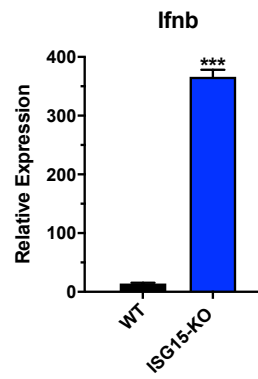
**A**



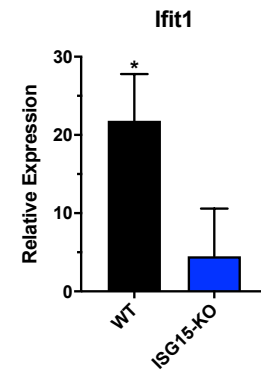
**B**



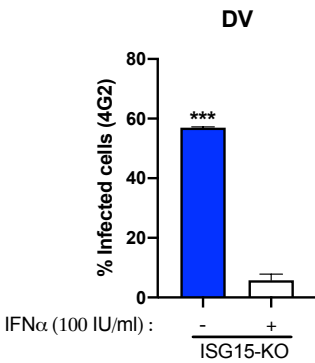
**C**



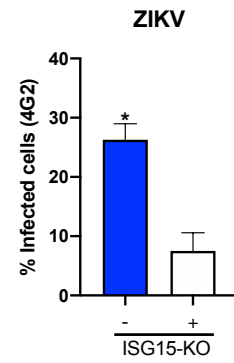
**D**



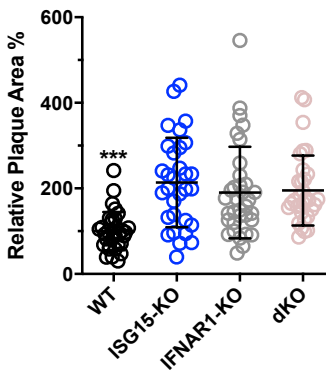
**E**



**F**



**G**



**H**

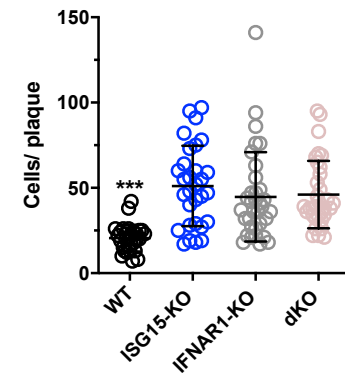


**Figure 5-Espada et al.**

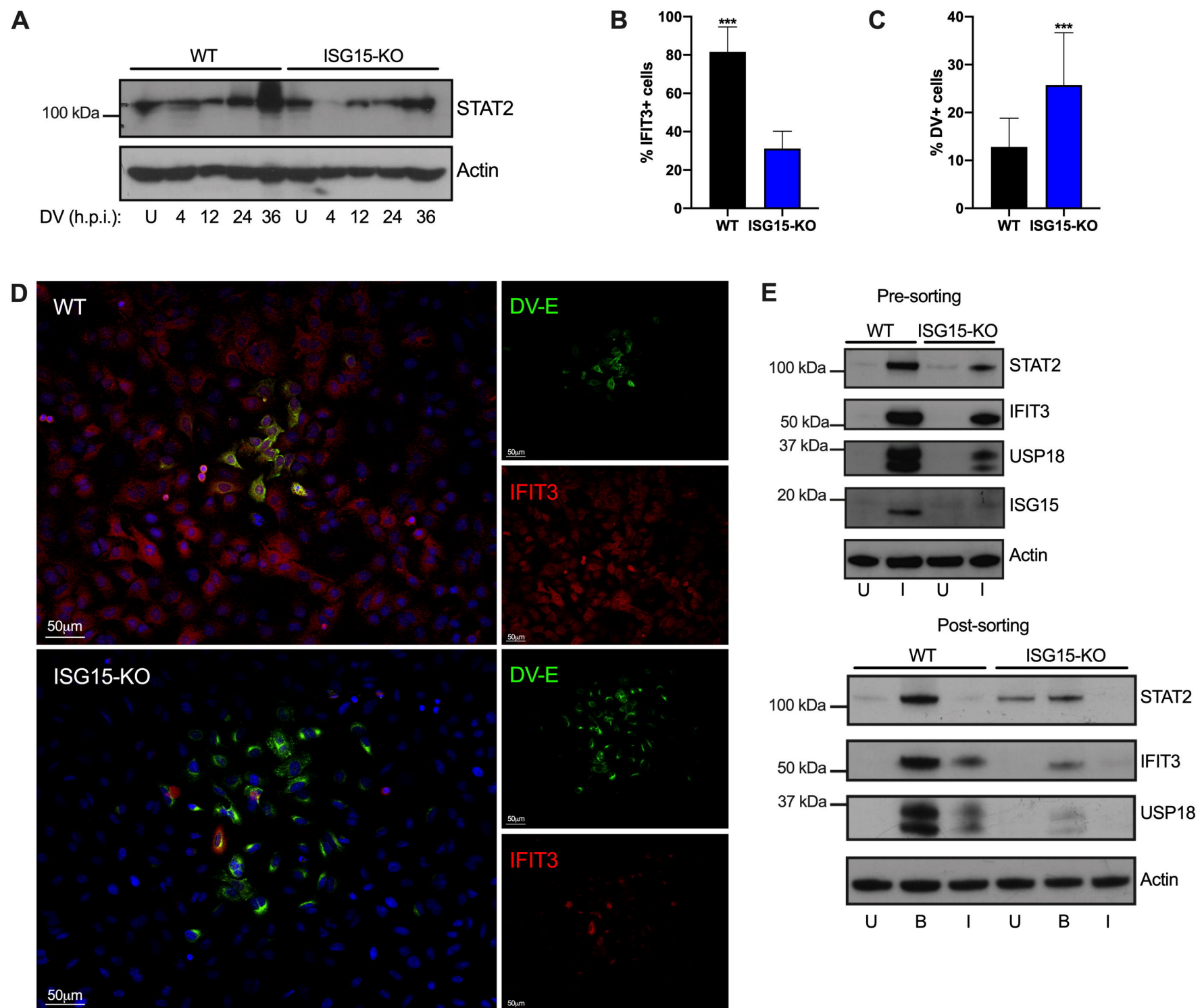


**Figure 6-Espada et al.**

